Nanocluster Formation in Electron-Irradiated Li_2O Crystals Observed by Elastic Diffuse Neutron Scattering

G. Krexner,[1] M. Prem,[2] F. Beuneu,[3] and P. Vajda[3]

[1]*Institut für Experimentalphysik, Universität Wien, Boltzmanngasse 5, A-1090 Vienna, Austria*
[2]*Laboratoire Léon Brillouin (CEA-CNRS), CEA Saclay, F-91191 Gif/Yvette, France*
[3]*Laboratoire des Solides Irradiés, Ecole Polytechnique (CEA-CNRS), F-91128 Palaiseau, France*

(Received 10 March 2003; published 23 September 2003)

Previous work performed on electron-irradiated Li_2O crystals has demonstrated the simultaneous formation of two populations of colloids of metallic lithium, one is associated with oxygen bubbles and a typical size of > 10 μm, while the other one consists of nanoclusters in the range of <10 nm. In the present neutron scattering investigation these small colloids are characterized in detail based on a thorough analysis of distortion scattering around Bragg peaks. It is shown that the small lithium colloids are slightly elongated precipitates with typical dimensions of around $\sim$5 nm. For the large lithium colloids a well-defined orientation relation with respect to the Li_2O matrix has been determined.

DOI: 10.1103/PhysRevLett.91.135502 PACS numbers: 61.72.Dd, 61.80.Fe, 61.82.Ms, 81.05.Je

Lithium oxide (Li_2O) is a prototype substance for both fundamental and applied investigations. As a highly ionic solid without d electrons it is a good target for first-principles electronic structure calculations (see, e.g., [1]), and for testing interatomic potentials required, e.g., for large-scale simulations of diffusion processes at high temperatures [2,3]. Being a superionic conductor, Li_2O is of interest in the context of solid state batteries [4], and as a tritium breeder it is regarded as a prospective candidate for first-wall materials in fusion reactors [5]. This latter aspect had initiated a major effort towards the investigation of radiation damage in Li_2O, especially by the research group at Japan Atomic Energy Research Institute, in which they studied the effects of γ rays, of neutrons, and of various ions upon its physical and physicochemical properties (see [5] for a review). More recently, it was discovered by two of the present authors that electron irradiation of Li_2O leads to the formation of metallic Li colloids as observed by conduction electron spin resonance (CESR) [6]. (Understanding and control of these colloids is important since their presence might, through the formation of LiT, interfere with the envisaged use of Li_2O as a tritium breeding material.) In fact, rather complete studies (via CESR, NMR, dielectric constant, and electron and optical microscopy) of electron-irradiated single crystals [7,8] have shown the presence of two types of Li colloids represented by, respectively, Dysonian- and Lorentzian-type CESR signals which can be associated with two different size distributions, one on the order of 10 μm and the other in the submicrometer range. Later, the luminescence of electron-produced Li colloids in Li_2O was investigated by Grishmanov *et al.* [9] while Vigreux *et al.* studied the bistable hysteresis (Overhauser effect) through CESR and electron-nuclear double resonance [10]. Finally, the simultaneous presence of molecular oxygen in disklike cavities associated with the large metallic colloids was established in a low-temperature magnetization study of irradiated Li_2O crystals [11].

Despite these results a more detailed analysis of the structure of the Li colloids and their arrangement within the Li_2O host lattice was still missing. After early attempts by x-ray and electron diffraction which were not successful due to the unfavorably low atomic number of Li, the low concentration of metallic Li produced by irradiation (10^{-3} to 10^{-2}) and the high ionicity of Li_2O, we decided to undertake a neutron scattering investigation on a triple-axis spectrometer. First results establishing the bcc structure of bulk Li for the large (micron-size) colloids were reported at a conference [12]. In addition, small-angle neutron scattering (SANS) measurements of another sample having undergone a different irradiation regime indicated the presence of small nonspherical precipitates with a typical size near 10 nm whose composition, however, could not be unambiguously identified. In what follows, we present a study of the distortion scattering observed in an irradiated single crystal of Li_2O leading to the conclusion that the small colloids are elongated clusters with typical diameters of around 5 nm.

Li_2O crystallizes in the cubic antifluorite structure with a lattice parameter $a = 0.461$ nm (space group $Fm\bar{3}m$). The specimen used was a 4×7 mm^2, 730 μm thick platelet (38.6 mg weight) obtained by cleavage along (111) from a float-zone grown single crystal of Li_2O. It had been irradiated with 1 MeV electrons from a Van de Graaff accelerator at 300 K, with a current of $\sim$40 μA/cm^2, to a dose of 15 C/cm^2. This provided an EPR spectrum similar to the ones discussed in Refs. [7,8] indicating the presence of both small and large Li colloids. The corresponding Li-metal concentrations as determined from the line intensities are, respectively, 2×10^{-5} and 2×10^{-3} per mole. The absence of any visible sign of the hyperfine split signal of the F^+ center

(oxygen vacancy + trapped electron) or of its nonmetallic clusters yields a detection limit of several 10^{-7} per mole.

The neutron investigations were performed on the triple-axis spectrometer VALSE at a cold-neutron guide of the Laboratoire Léon Brillouin. Measurements were performed at room temperature, mostly at a wavelength of 0.292 nm with the analyzer set into the second order position. The use of an analyzer crystal in contrast to the more common diffractometer setup led to effective discrimination of inelastic scattering (energy resolution <0.5 meV) and made corrections for resolution in Q space (< 0.01 Å^{-1} for radial scans) negligible. A nonirradiated crystal of similar dimensions served as a reference. The scattering plane was (110) providing access to Bragg peaks of types (111), (200), and (220).

Figure 1 compares radial scans along [111] and [100] directions through, respectively, the (111) and (200) Bragg peaks of the irradiated and the nonirradiated crystal. In addition, large rectangular areas around the Bragg positions were scanned in order to obtain two-dimensional maps of the intensity distribution. Figure 2 shows the scattering pattern measured around the (111) peak demonstrating that the additional intensity is not only observed radially along [111], but it covers a broad area extending in all directions around the peak position. The scattering patterns around the (200) and (220) peaks are qualitatively similar. Further, the irradiation process induced a slight increase of the lattice parameter (implying an interstitial-type defect) leading to a relative change in the crystal volume $\Delta V/V \sim 3\Delta a/a = (7 \pm 1.5) \times 10^{-4}$.

By performing an expansion of the elastic scattering amplitude arising from pointlike defects and the displaced atoms in its neighborhood, it is possible to decompose the scattering intensity in several terms containing specific information on the concentration, strength, and size of the defect (for an introduction, see, e.g., [13]; a rigorous treatment can be found in [14]. The term pointlike is used to summarize all of the defects inducing

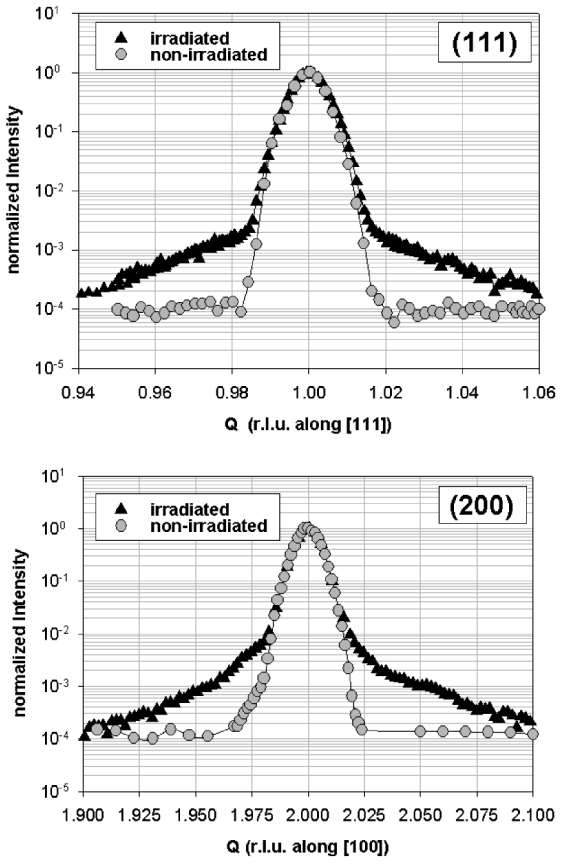

FIG. 1. Comparison of the scattering intensity (on a logarithmic scale) observed in irradiated and nonirradiated Li_2O along radial scans through the (111) and (200) peaks. In the reference sample the peak shape is a Gaussian upon a flat background while distortion scattering is clearly visible after electron irradiation. The intensities have been normalized to facilitate comparison. The momentum transfer Q is given in reciprocal lattice units $2\pi/(a\sqrt{h^2 + k^2 + l^2})$.

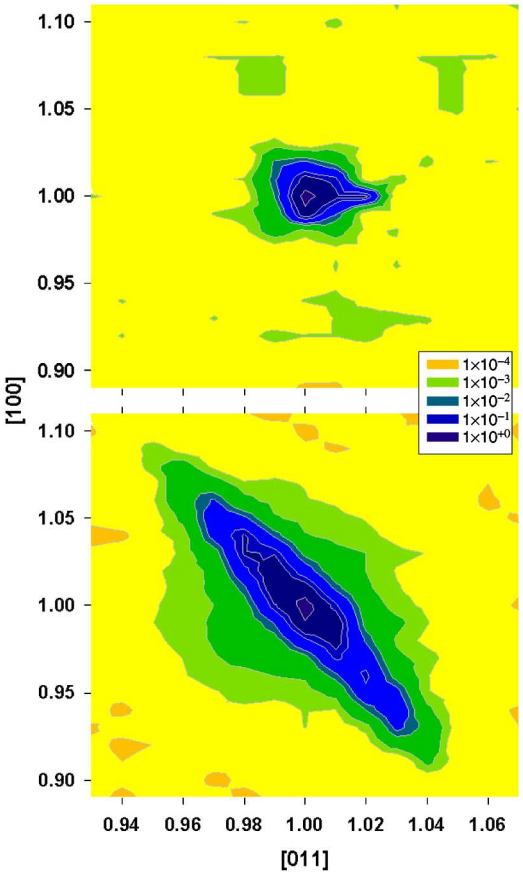

FIG. 2 (color online). Normalized isointensity contours of elastic diffuse scattering around the (111) peak of an nonirradiated (top) and an irradiated (bottom) crystal of Li_2O. Units are defined as explained in the caption of Fig. 1. No lines of zero intensity are observed in the intensity distribution of the distortion scattering in the irradiated sample.

displacements decreasing as C/r^2 similar to true point defects such as vacancies or single interstitial atoms. C is usually termed "defect strength." For further discussion, cf., e.g., [15]). Close to the Bragg peak the elastic diffuse scattering intensity $S(\mathbf{q})$ can be written as a sum of a symmetric term $S_{\mathrm{sym}}(\mathbf{q}) = (1/2)[S(\mathbf{q}_+) + S(\mathbf{q}_-)]$ and an antisymmetric term $S_{\mathrm{anti}}(\mathbf{q}) = (1/2)[S(\mathbf{q}_+) - S(\mathbf{q}_-)]$ (the reduced vector $\mathbf{q} = \mathbf{Q} - \mathbf{H}$ is defined as the difference between the scattering vector $\mathbf{Q}$ and the reciprocal lattice vector $\mathbf{H}$ at the center of the Brillouin zone; $\mathbf{q}_+$ and $\mathbf{q}_-$ refer to values of $\mathbf{q}$ corresponding to $\mathbf{Q}\cdot\mathbf{H} > H^2$ and $\mathbf{Q}\cdot\mathbf{H} < H^2$, respectively). The symmetric part, usually denoted as Huang scattering, is described by the following expression where the quantities n_{cl}, c_d, and $\Pi^{(i)}$ contain information on the defect; b, Ω, and $\gamma^{(i)}$ are related to properties of the matrix; and H and q are defined by the scattering geometry:

$$S_H(q) = n_{\mathrm{cl}} c_d \frac{b^2}{\Omega^2}\frac{H^2}{q^2}[\gamma^{(1)}\Pi^{(1)} + \gamma^{(2)}\Pi^{(2)} + \gamma^{(3)}\Pi^{(3)}]. \tag{1}$$

Here, b and Ω denote the mean coherent neutron scattering length and the atomic volume, the $\gamma^{(i)}$ contain combinations of the elastic constants of the matrix depending on the angle between $\mathbf{H}$ and $\mathbf{q}$, n_{cl} is the number of single defects forming a cluster ($n_{\mathrm{cl}} = 1$ in the case of a single interstitial or vacancy), c_d denotes the concentration of defects independent of whether they have agglomerated in clusters or not, and the $\Pi^{(i)}$ can be expressed in terms of the dipole force tensor P_{ij} associated with a single defect ("dipole" refers to the first term of a multipole expansion of the elastic force field): $\Pi^{(1)} = (1/3)(\mathrm{Tr}P)^2$, $\Pi^{(2)} = (1/6)\Sigma_{i>j}(P_{ii} - P_{jj})^2$, and $\Pi^{(3)} = (2/3)\Sigma_{i>j}P_{ij}^2$. While $\Pi^{(1)}$ is a measure of the defect strength, information on the defect anisotropy is provided by $\Pi^{(2)}$ and $\Pi^{(3)}$. The antisymmetric term is an interference term which turns out to be close to zero in the present case and, therefore, is not discussed any further.

At a greater distance from the Bragg point an expression for the asymptotic diffuse scattering intensity [also termed Stokes-Wilson (SW) scattering] can be derived:

$$S_{\mathrm{SW}}(q) = c_d \frac{b^2}{\Omega^2}\frac{1}{4\pi\gamma B}\sqrt{\frac{\Pi^{(1)}}{3}}\frac{H}{q^4}\Phi(\mathbf{q},\mathbf{H}), \tag{2}$$

where B is the bulk modulus of the crystal, γ is the Eshelby constant defined as $3(1-\nu)/(1+\nu)$ with ν denoting Poisson's ratio ($\nu \sim 0.168$ and $\gamma \sim 2.14$ for Li_2O), and Φ is a function depending on the angle between $\mathbf{q}$ and $\mathbf{H}$ amounting to $128\pi^3/27$ for the radial scans evaluated below. Another important relation exists between the measured volume change and the defect strength:

$$\frac{\Delta V}{V} = \frac{c_d}{B}\sqrt{\frac{\Pi^{(1)}}{3}}. \tag{3}$$

Both Eqs. (2) and (3) contain information on c_d and $\Pi^{(1)}$; Eq. (1) contains information on c_d, combinations of the $\Pi^{(i)}$ and, in addition, n_{cl}. In principle, scans through the Bragg peaks can be chosen along transverse directions which involve only one of the $\Pi^{(i)}$ at a time so that these quantities can be determined separately. In the present case the mosaic width of the crystal had increased strongly during the irradiation process so that only a qualitative picture could be derived from transverse scans (cf. Fig. 2). The respective combinations of $\gamma^{(i)}\Pi^{(i)}$ needed for a quantitative evaluation of the radial scans are $[1/(3c_{11}^2)](\Pi^{(1)} + 2\Pi^{(2)})$ along [100], $\{2/[3(c_{11} + c_{12} + 2c_{44})^2]\}(2\Pi^{(1)} + \Pi^{(2)} + 3\Pi^{(3)})$ along [110] and $[3/(c_{11} + c_{12} + 2c_{44})^2](\Pi^{(1)} + 2\Pi^{(3)})$ along [111]. The elastic constants were taken from Ref. [16].

Figure 3 shows the Huang and asymptotic scattering observed radially close to two peaks. The details of the intensity decrease that are observed beyond the Huang region depend strongly on the type of defect giving rise to this scattering; however, the particular combination of (-4) and $(-10/3)$ for $S(\mathbf{q}_-)$ and $S(\mathbf{q}_+)$, respectively, has been found previously in numerical simulations to be typical for spherically symmetric defect clusters in an isotropic medium [17]. The value $q = q_c$ where the crossover of the -2 and the -4 range takes place can be interpreted in terms of a characteristic radius of the underlying defect $R_c \sim 1/q_c$. Typical diameters of the defect clusters along the crystallographic directions [011], [$0\bar{1}1$], and [100] were obtained by numerical fits to the data giving $\sim 8 \times 8 \times 4$ nm, to $\pm 20\%$ for each

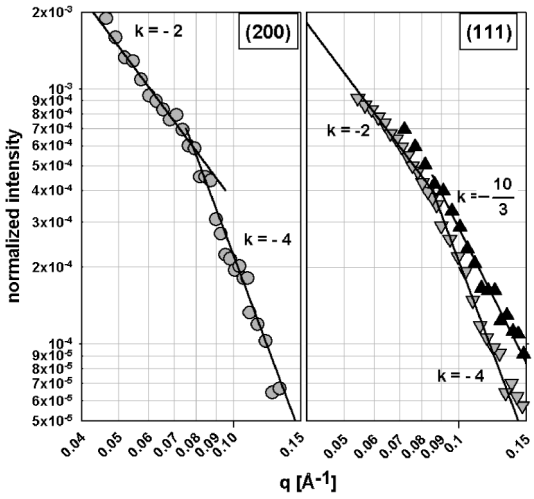

FIG. 3. Radial part of the scattering intensity on a doubly logarithmic scale as a function of $q = |\mathbf{Q} - \mathbf{H}|$, where $\mathbf{H}$ stands for the reciprocal lattice vectors [200] and [111] in Fig. 1. For the (200) peak the symmetrized intensity is displayed showing the characteristic slope $k = -2$ for the Huang region followed by -4 for SW distortion scattering. For the (111) peak the slope for SW scattering on the $\mathbf{q}_-$ side (∇) is likewise -4 while the exponent $-10/3$ is found on the $\mathbf{q}_+$ side ($\blacktriangle$) (see text).

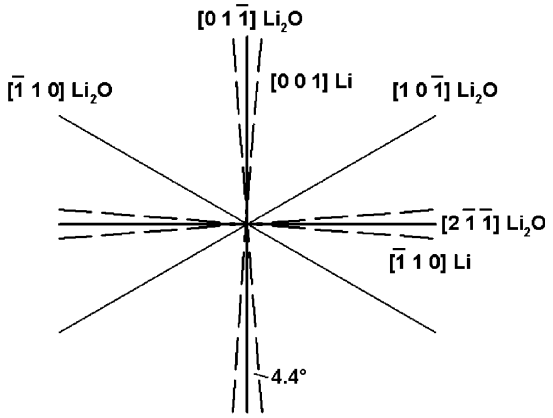

FIG. 4. Shown is a (111) plane of Li_2O coinciding with a (110) plane of the large Li colloids. The orientation relation is defined by $[\bar{1}10]_{Li} \parallel [2\bar{1}\,\bar{1}]_{Li_2O} \pm 4.4°$ (two variants) and $[001]_{Li} \parallel [01\bar{1}]_{Li_2O} \pm 4.4°$ (again two variants). The orientation relation $[110]_{Li} \parallel [111]_{Li_2O}$ holds perpendicularly to the plane shown.

dimension. This is in good accordance with a small-angle scattering investigation of the same sample (data not shown here) yielding an averaged Guinier radius of $\sim$2.5 nm corresponding to a mean geometrical diameter of about 6.5 nm and leading to $n_{cl} \sim 10\,000$ for the number of atoms in one cluster (the SANS data do not permit a unique determination of the cluster shape since the scattering pattern is obtained by averaging various possible orientations). In order to obtain absolute scattering cross sections the measured intensities were calibrated with the incoherent scattering of a vanadium standard. Then, the set of Eqs. (1)–(3) were evaluated in order to determine the $\Pi^{(i)}$ and the defect concentration c_d. It was found that $\Pi^{(1)} \sim 1 \times 10^{-35}(\mathrm{Nm})^2$, $\Pi^{(2)}/\Pi^{(1)} \sim 0.3$, $\Pi^{(3)}/\Pi^{(1)} \sim 0.3$, and $c_d \sim 3 \times 10^{-5}$ where we estimate the uncertainty in these quantities to lie within a factor 2–3. Since the $\Pi^{(i)}$ represent quadratic invariants of the dipole force tensor there is no unique solution for the tensor components. However, the symmetry properties of the scattering show that the defect symmetry can be at most orthorhombic. In addition, model calculations (not shown here) based on tensors whose components respect the constraints set by the $\Pi^{(i)}$ found in the experiment are in good agreement with the observed distribution of diffuse scattering around the Bragg peaks. The surprisingly large values obtained for the $\Pi^{(i)}$ suggest conditions of high pressure inside the small colloids, which can be related to the fact that the atomic volume of metallic Li is nearly twice as large as for the ionic state of Li in the oxide.

The above results confirm the existence of a population of small Li colloids established in earlier CESR experiments whose results are compatible with respect to both concentration and size. The existence of a narrow distribution of small Li clusters suggests a stable intermediate stage on the way from the formation of isolated atomic species, as an immediate effect of irradiation, to the large Li colloids and the associated oxygen bubbles.

Finally, we turn to the lattice orientation of the large metallic precipitates with respect to the Li_2O matrix. A set of well-defined diffraction peaks could be observed in additional measurements beyond those presented in [12] yielding the crystallographic relations presented in Fig. 4. The observed formation of orientational variants around principal symmetry directions in order to accommodate the lattice mismatch between the matrix and precipitate has been observed also in the low-temperature transition of elemental metallic Li [18]. There is no indication of strong displacement fields generated by the large colloids around which strain relaxation must have occurred already at a much earlier stage.

To summarize, we have identified a distinct population of nanoclusters generated in Li_2O during electron irradiation, which may be regarded as relatively stable precursors to the formation of the larger micron-size colloids described earlier. These clusters are characterized regarding their size, concentration, shape, defect strength, and the number of atoms contained on the average. In addition, the orientation relation of the large Li colloids with respect to the oxide matrix has been fully determined.

[1] S. Albrecht, G. Onida, and L. Reining, Phys. Rev. B **55**, 10 278 (1997).
[2] H. Pfeiffer, J. Sanchez-Sanchez, and L. J. Alvarez, J. Nucl. Mater. **280**, 295 (2000).
[3] J. G. Rodeja, M. Meyer, and M. Hayoun, Model. Simul. Mater. Sci. Eng. **9**, 81 (2001).
[4] Y. Oishi *et al.*, J. Nucl. Mater. **87**, 341 (1979).
[5] N. Roux, C. Johnson, and K. Noda, J. Nucl. Mater. **191/194**, 15 (1992).
[6] P. Vajda and F. Beuneu, Phys. Rev. B **53**, 5335 (1996).
[7] F. Beuneu and P. Vajda, Phys. Rev. Lett. **76**, 4544 (1996).
[8] F. Beuneu *et al.*, Phys. Rev. B **55**, 11 263 (1997).
[9] V. Grishmanov *et al.*, Nucl. Instrum. Methods Phys. Res., Sect. B **134**, 27 (1998).
[10] C. Vigreux, L. Binet, and D. Gourier, J. Phys. Chem. B **102**, 1176 (1998).
[11] F. Beuneu *et al.*, Phys. Rev. Lett. **83**, 761 (1999).
[12] P. Vajda *et al.*, Nucl. Instrum. Methods Phys. Res., Sect. B **166/167**, 275 (2000).
[13] P. Ehrhart, J. Nucl. Mater. **216**, 170 (1994).
[14] P. H. Dederichs, J. Phys. F **3**, 471 (1973).
[15] M. A. Krivoglaz, *X-Ray and Neutron Diffraction in Nonideal Crystals* (Springer, Berlin, 1996).
[16] S. Hull *et al.*, J. Nucl. Mater. **160**, 125 (1988).
[17] S. Iida *et al.*, J. Mater. Res. **3**, 267 (1988).
[18] O. Blaschko *et al.*, Phys. Rev. B **59**, 9095 (1999).